Review | Vol. 9, No. 1 | 1 Jan 2019 | OPTICAL MATERIALS EXPRESS 112
Optical Materials EXPRESS

Herding cats: managing gold atoms on common transparent dielectrics [Invited]

ADRIANNA MILEWSKA,[1,2] ARNI S. INGASON,[3] OLAFUR E. SIGURJONSSON,[4,5] AND KRISTJAN LEOSSON[1,6,*]

[1]*Innovation Center Iceland, Arleynir 2-8, IS112 Reykjavik, Iceland*
[2]*School of Engineering and Natural Sciences, University of Iceland, Sæmundargata 2, IS101 Reykjavik, Iceland*
[3]*Grein Research ehf. Dunhaga 5, Reykjavik, Iceland*
[4]*The Blood Bank, Landspitali The University Hospital of Iceland, Snorrabraut 60, IS105 Reykjavik, Iceland*
[5]*School of Science and Engineering, Reykjavik University, Menntavegur 1, IS101 Reykjavik, Iceland*
[6]*Science Institute, University of Iceland, Dunhaga 5, IS107 Reykjavik, Iceland*
**kristjan.leosson@nmi.is*

Abstract: Simple methods to control the self-organization of gold atoms on commonly employed transparent dielectrics are presented. On one hand, surface diffusion of gold atoms can be suppressed to a sufficient degree as to realize ultra-thin (as low as approximately 5 nm) void-free semi-transparent conducting gold films over macroscopic areas while, on the other hand, their high surface mobility can be harnessed to fabricate large-area substrates compatible with cell culturing and imaging, having widely tunable field-enhancement properties for surface-enhanced Raman scattering.

1. Introduction

Systematic optical studies of thin gold films and gold nanoparticles can be traced back at least as far as to Faraday's experiments at the Royal Institution of Great Britain in the 1850s [1]. Faraday prepared beaten gold leaf that he estimated to have an average thickness of 90 nm and stated that "we are satisfied that it is truly transparent where the gold is continuous, and that the light transmitted is green." In addition, he indicated that "by chemical means, the film may be attenuated to such a degree as to transmit a ray so luminous as to approach to white, and that in parts [of the gold leaf] which have every appearance of being continuous in the microscope." Faraday also prepared gold particles "too small to be recognized by the highest powers of the microscope" and found that "the transmitted tint became ruby or violet-ruby." After performing annealing experiments on his samples, Faraday concluded that it was "evident that all the colours described are produced by one and the same substance, namely gold, the only apparent difference being the state of division and different degrees of the application of heat" [1]. A few years before, Sir William Robert Grove had observed that thin metal films of different metals could be deposited by ion impingement on metallic cathodes (now referred to as sputtering) [2] and with further developments in physical vapor deposition and, later still, the introduction of X-ray diffraction and electron and scanning probe microscopy techniques, studies of the optical properties of thin metal films and their relationship to structural and electrical properties became a major field of research, especially after the mid-20th century [3]. Gold has always attracted particular attention because of its chemical stability, most notably in the last three decades with its application in surface-enhanced Raman scattering (SERS) and plasmonics [4], its optical properties being second only to silver [5], which is less chemically stable. At the beginning of the 21st century, advances in nanometer-scale engineering have opened up new opportunities for metal optics, such as the tailoring of optical properties of (meta)surfaces by patterning of thin metal films [6], carving of optical nanostructures out of atomically-flat single-crystal metals [7] and

#346724 https://doi.org/10.1364/OME.9.000112
Journal © 2019 Received 16 Oct 2018; revised 26 Nov 2018; accepted 26 Nov 2018; published 10 Dec 2018

Optical Materials EXPRESS

harnessing of quantum and non-linear effects [8], to name a few examples. Furthermore, there has been increased focus on the study of ultra-thin (<10 nm) metal films (UTMFs), e.g., related to their applications in plasmonics [9] and optoelectronic devices [10].

The structural development of gold films during deposition on glass or similar materials follows a predictable pattern of island nucleation, island growth, coalescence and eventually the filling of voids and formation of a structurally continuous film [11]. The number and size distribution of nucleated islands as well as the precise deposition thickness at which coalescence and continuity occur depends, in general, on the deposition method and deposition parameters as well as on the type, temperature and surface preparation of the substrate. Around the percolation threshold (the point at which a film of disconnected islands develops into a network with long-range connectivity), a sharp increase in statistical fluctuation of the optical density of states is observed [12], correlated with local electric field enhancement and a range of interesting optical phenomena [13–15]. For gold films, even above the continuity threshold, the exact value of the complex dielectric function of the deposited material will, in general, depend on the method of preparation [16]. In this context, accurate methods for determining the physical structure of thin films, independent of their optical or electrical properties, such as measurements of X-ray reflectivity (XRR), are highly advantageous. Discontinuous films, on the other hand, exhibit a structure-dependent and anisotropic dielectric function that is not adequately described by commonly used effective-medium approximation methods [17]. Finally, it must be kept in mind that the dielectric function is a classical concept that does not account for, e.g., spatial nonlocality, which may have significant consequences at the nanometer scale and below [18]. These facts, in addition to inaccuracies in some of the tabulated literature data of the dielectric function of gold over the past decades [16], mean that the premises of comparison between theory or numerical simulations and experiment must always be carefully considered.

On dielectric substrates commonly used in plasmonics research (such as glass, thermal oxide, fused silica/quartz, thermosetting polymers), gold atoms exhibit high mobility, even at room temperature, and the deposited material therefore self-organizes into an energetically favorable state, i.e. either a discontinuous or continuous film, depending on the amount of material deposited. In the present paper, we will review some simple fabrication techniques that have been reported in recent years with the aim of giving researchers increased control over this self-organizing behavior of gold films for tuning the morphology and optical properties of such films on transparent dielectrics. These methods involve only standard cleanroom technologies and neither special substrates or deposition conditions nor metallic adhesion or seeding layers that can compromise the optical, electronic and physical properties of the overall structure [19–21]. In particular, we will consider, on one hand, the fabrication of ultra-thin gold films for use as semitransparent electrodes and, on the other hand, ripening effects in structured and disordered films functioning as SERS substrates compatible with cell growth.

2. Ultra-thin structurally continuous gold films

For a long time, it was considered “conventional wisdom” in the field of metal optics that fabricating structurally continuous gold layers on glass substrates below a film thickness of about 15 nm was not possible with standard cleanroom fabrication methods. Indeed, this was shown to be the case even on silanized glass, where (3-mercaptopropyl)trimethoxysilane (MPTS) was used to improve adhesion of gold islands on a glass surface [22]. In contrast, metallic seeding layers can lower the percolation threshold to as low as 1 nm [23]. Recently, however, it was shown that on the glassy optical polymer benzocyclobutane (BCB), a well-known material for thin-film applications [24], the deposition thickness at which island coalescence and continuity were observed was significantly lowered, as compared to gold deposited on clean glass substrates under identical conditions [25]. The maximum optical transmission of a structurally continuous gold film deposited on BCB (including also the ≈4%

Optical Materials EXPRESS

incoherent reflection from the backside of the underlying substrate), corresponding to a deposition thickness as low as 7-8 nm, was close to 70% in the green-yellow wavelength range in accordance with the theoretically predicted shape of the transmission curve (and Faraday's observations mentioned above). However, the absolute level of transmission across the whole 400-1000 nm wavelength range for the film was lower than expected for a (hypothetical) structurally perfect layer (assuming bulk-like dielectric properties derived from thicker deposited films). The sheet resistance of the 7-8 nm-thick gold film on BCB was found to be below 20 Ω/sq, only slightly higher than that reported for epitaxial gold of the same thickness [25].

An even more pronounced suppression of the coalescence and continuity thresholds (to <3 nm and ≈5 nm, respectively) was observed on MPTS-coated fused silica substrates where gold was deposited at moderate evaporation rates (1 Å/s) using conventional electron-beam evaporation [26]. In this case, a significant change in film morphology as compared to thermally deposited gold of the same deposition thickness on identically prepared substrates was observed and attributed to the MPTS layer being subject to high-energy radiation prior to gold deposition, originating from the deceleration of the (7.5-kV) electrons impinging on the source material. In order to assess the structural properties of the film above the continuity threshold, XRR measurements were carried out on such samples and fitted with a two-layer model for the gold film, keeping the thickness and density of each layer as free fitting parameters. The lowest deposition thickness giving a void-free film was found to be just over 5.4 nm and its XRR curve is shown in Fig. 1. Fitting the measured data with the two-layer model yielded a density (thickness) of 19.3 g/cm^3 (3.4 nm) for the lower layer and 17.3 g/cm^3 (2.3 nm) for the upper layer, confirming that a layer of bulk gold density (ρ_{Au} = 19.32 g/cm^3) has formed on the fused silica surface at this deposition thickness, capped by an effectively less dense (≈90%) layer of surface roughness. These XRR-measured density values of continuous films were found to be stable at room temperature for up to 6 months (cf. Ref [26], supporting information).

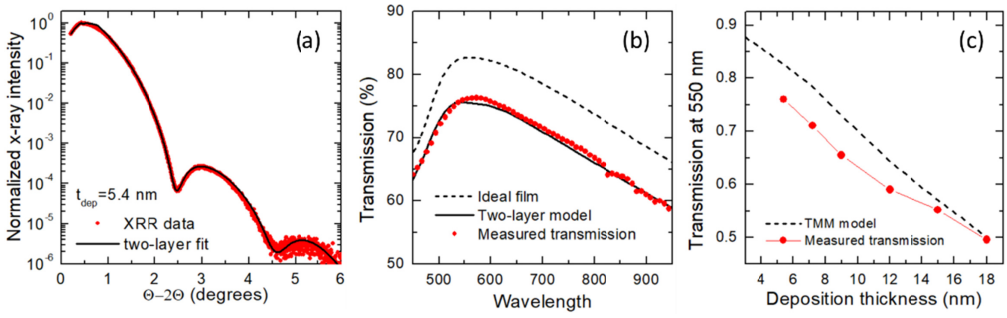

Fig. 1. (a) XRR measurements (red symbols) for a gold film of 5.4 nm deposited thickness on an activated fused silica substrate. A good fit to the measured data (black line) is obtained with a two-layer model for the gold film, where the lower layer is characterized by the bulk density of gold. (b) Optical transmission of the same film, showing a discrepancy between the measured data (red symbols) and the idealized transmission curve (dashed line) that can be accounted for by introducing graded interfaces in the model (solid line). (c) The idealized gold transmission at 550 nm (dashed line) compared to measured data (red symbols).

Similar to the gold-coated BCB discussed above, optical transmission of structurally continuous gold films was lower than expected from calculations based on the transfer-matrix method (TMM) that presuppose a structurally perfect film with bulk-like dielectric properties. Such models were, however, found to be fully adequate at larger deposition thickness (see Ref [25]. and Supporting Information for Ref [26].). The difference between calculated and measured optical transmission was found to be approximately constant across the 400-1000 nm wavelength range for a given thickness of the structurally continuous film, indicating that the reduction is not caused by residual plasmonic absorption due to film imperfections (voids,

Optical Materials EXPRESS

cracks, roughness). An acceptable agreement between theory and experiment was obtained, however, by assuming graded rather than sharp transitions in the dielectric function at the gold-air and gold-substrate interfaces in the transfer-matrix model. A similarly graded transition could also be used to account for observed propagation losses of long-range surface plasmon polaritons in ultra-thin gold stripe waveguides embedded in a dielectric [27]. This further illustrates the pitfalls of fitting optical data without additional structural information, as the measured transmission curves in Ref [26]. could have been reasonably well fitted with a simple model of a perfect gold film by assuming a larger gold thickness than was actually deposited. It should be noted that the observed reduction in optical transmission puts a limit on the maximum transparency of ultra-thin gold films that can be expected in conventionally deposited films (cf. Figure 1).

3. Utilizing gold surface mobility for controlling particle size and spacing

After vacuum deposition of gold films, rearrangement of gold atoms can be observed to take place for days after deposition when samples are stored at room temperature [25]. Below the coalescence threshold, films tend towards increased segregation in individual islands while above the threshold, rearrangement of gold atoms may improve film quality, reflected, e.g., in an observed reduction in sheet resistance with time. Increasing sample temperature obviously speeds up this process and results in differently shaped island or percolating film patterns [22]. Contrary to the case of semi-transparent metal films discussed above, where plasmonic excitation should ideally be eliminated, applications in surface-enhanced Raman scattering require absorption of incident laser light by the metal film, coupled with a suitable nanometer-scale structure to maximize local field enhancement [28]. In particular, small gaps between metal nanoparticles lead to strong local SERS enhancements, mirroring the electrostatics of coupled metal structures [29]. Strong local fields ("hotspots") do not, however, necessarily lead to homogeneous overall SERS enhancement across macroscopic areas for practical applications, without a sufficient density of spots and proper statistical distribution of their intensity [30]. Furthermore, a narrow-band resonance is not optimal as the SERS signal scales with the squares of the local electric field amplitudes at the excitation and emission wavelengths, which may easily be separated by 100 nm (e.g. for excitation at 633 nm and a 2000 cm^{-1} spectral range). It is therefore often misleading to assume an E^4-dependence of the SERS effect in plasmonic structures since a given hotspot will rarely give strong field enhancement for both excitation and Stokes wavelengths.

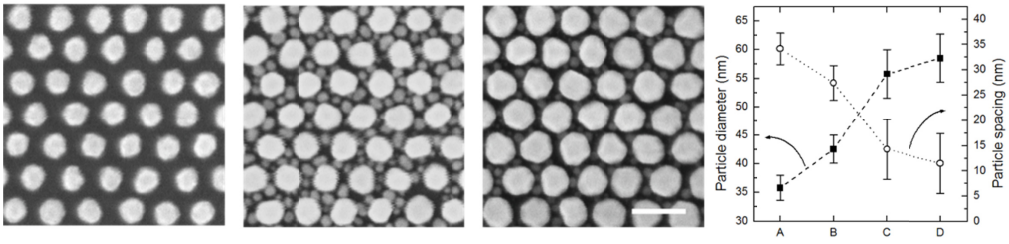

Fig. 2. Patterned gold particles (left SEM image) on a thermally oxidized Si surface (100 nm oxide thickness) ripened by repeated deposition and annealing of thin (< = 6 nm) gold layers (middle and right SEM images). The recrystallization of the gold particles is also clearly seen from appearance of facets in the annealed structure. Scale bar is 100 nm. The plot shows development of average diameter and minimum spacing of the initially patterned particles, A, at subsequent processing steps, B, C and D (step D not shown, further details can be found in Ref [27].).

Realizing small (< = 10 nm) gaps between patterned metal particles is a challenge for most conventional lithographic patterning methods. For properly designed structures, the high surface mobility of gold can, however, be used as a post-patterning tool to reduce interparticle spacing, as shown in Fig. 2. In Ref [31], a templated particle growth method was introduced

Optical Materials EXPRESS

whereby patterned gold nanoparticles were ripened with additional gold deposition and annealing, i.e. where smaller nanoislands were eventually consumed by bigger ones during the annealing phase (akin to Ostwald ripening of crystals in solid solution [32]). Numerical simulations indicated that this resulted in a broad-band field enhancement, about 1-2 orders of magnitude higher than that observed in the originally patterned structure where enhancement also mainly occurred in a relatively narrow wavelength range around the localized plasmon resonance wavelength of the particles, as expected. The final structure resulted in a uniform measured SERS enhancement up to $\approx 4 \times 10^6$, three orders of magnitude higher than the originally patterned structure, for excitation at 633 nm and detection at -1620 cm^{-1} (705 nm).

Other methods have been used for realizing small gaps between metallic particles for SERS detection, including metal deposition on high-aspect-ratio structures such as leaning nanopillars [33] or deposition into self-assembled 3D networks like paper [34] or anodized aluminum oxide [35]. While such structures are suitable for detecting particular analytes in solution they are not compatible with other applications, notably cell growth, where ultra-thin metal films with a high density of hotspots (on the length scale of the cell) across large areas are more convenient, preferably deposited on glass or other transparent and biocompatible substrates for allowing inverted-microscope investigation and Raman imaging. Naturally, in such a case, SERS enhancement will only be observed for molecules at the cell membrane where the cells attach to the substrate, as opposed to e.g. SERS from within the cell that can be observed after internalization of nanoparticles or nanoparticle clusters (provided that those particles end up in positions of interest within the cell) [36,37]. Measurements of Raman spectra at cell membranes using SERS-active cell-culture substrates may, however, provide a useful non-invasive tool, e.g., for using mineralization on the cell surface for monitoring the stage of differentiation of bone-marrow mesenchymal stromal cells (MSCs) that differentiate into cells of the connective tissue lineage, such as adipocytes, osteoblasts and chondrocytes.

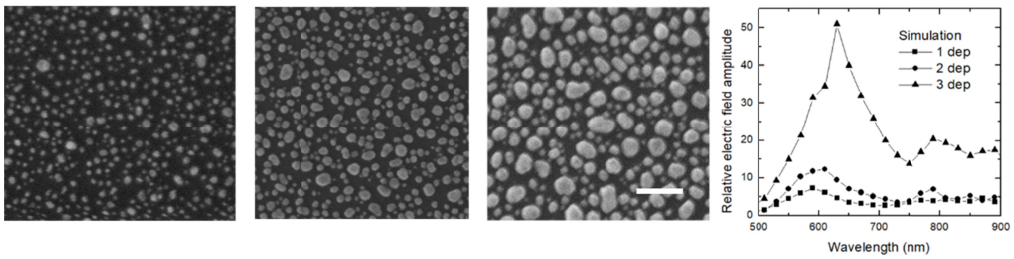

Fig. 3. Self-organized gold islands fabricated by successive deposition and annealing of ultra-thin gold layers (1,2 and 3 cycles, respectively) on thermally oxidized silicon substrates. Scale bar is 100 nm. The plot shows the maximum amplitude of the local electric field between islands relative to the incident field, as determined by a numerical (FDTD) simulation of a similar structure of gold islands.

During investigations of the process of ripening pre-patterned metal particles mentioned above it also became clear that substantial field enhancements were observed in non-patterned areas, i.e. where only repeated deposition and annealing of ultra-thin gold layers had taken place, although the resulting SERS enhancement was not as large as in the patterned areas [31]. The procedure is, however, much simpler as it does not involve high-resolution lithography and can be readily used to cover arbitrarily large substrates. A comparable fabrication approach was also independently developed by other authors [38]. In order to demonstrate the potential of this method, we used thin-film nanostructures produced by successive steps of gold deposition (≈4 nm) and annealing (at 350°C) without pre-patterning in order to fabricate large-area SERS substrates having a wide random distribution of island sizes, ranging from below 5 nm to above 40 nm equivalent diameter, as shown in Fig. 3. For reference, we performed finite-difference time-domain (FDTD) simulations on hemispherical island structures having the same placement and size distribution as the actual structures, thus

Optical Materials EXPRESS

also taking into account the variation in island height (using data for the gold dielectric function from Olmon et al. [16]). While there is not an exact correspondence between the real and the simulated structures, due to limitations of the simulation software and the imaging techniques, such simulations still provide some insight into the development of the pattern of field enhancement after the different processing steps and potential co-location of hotspots at different wavelengths. The wavelength-dependent field enhancement derived from FDTD simulations is shown in the plot on Fig. 3.

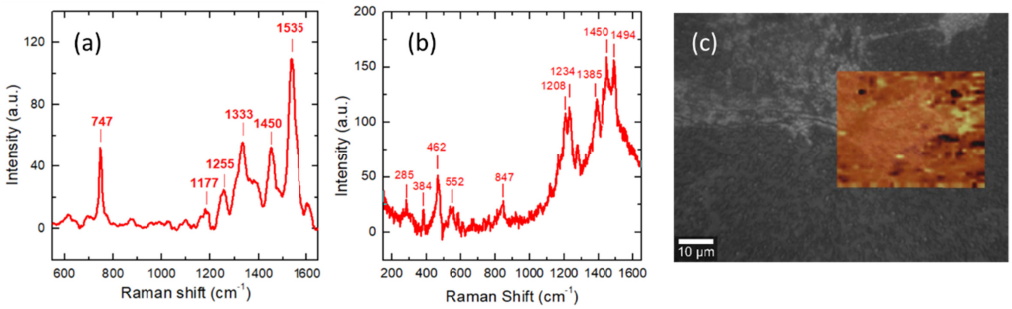

Fig. 4. (a) Rhodamine 6G spectrum recorded on a gold film substrate with randomly arranged nanoparticles prepared with three cycles of deposition and annealing as described in the text and shown in Fig. 3. (b) Raman spectrum from a fixed undifferentiated MSC cultured on a gold nanoparticle film. The broad background signal from 1100 to 1600 cm^{-1} originates from the glass substrate. (c) Raman image (462 cm^{-1} band) overlaid on an optical microscope image of the MSCs.

We investigated the variation of the Raman scattering signal on substrates prepared by multiple deposition and annealing of ultra-thin gold layers by imaging the 1535 cm^{-1} of Rhodamine 6G (see Fig. 4(a)) uniformly dispersed on the surface, using a confocal WITec Alpha 300 Raman imaging system. The spatially-dependent intensity variation of this peak exhibited a normal distribution with $\sigma = 7\%$ (633-nm excitation wavelength, NA = 0.9, 2500 measurement points at 300-nm intervals). Furthermore, we tested the compatibility of the substrates with MSC growth, confirming that cells proliferated on the SERS substrates and that Raman signals that correlated with the cell attachment to the surface were detected (Figs. 4(b) and (c)). Further work is needed to conclusively identify the molecular origin of those signals. Details of the cell preparation, Raman imaging and numerical simulations will be published elsewhere.

4. Conclusions

In summary, we have reviewed how simple cleanroom processing techniques, such as substrate silanization and irradiation, as well as successive gold deposition and thermal annealing, can be used to control the self-organizing behavior of gold atoms on commonly used dielectric substrates, by either suppressing or enhancing gold surface mobility. Furthermore, we have shown how comparison between theory and experiment is often problematic when assuming idealized structures and bulk-like properties of the gold dielectric function, as such assumptions are generally not justified at the nanometer scale.

Funding

Icelandic Research Fund (163417-051).

Acknowledgements

The authors thank A. Kossoy, V. Merk, J. Kneipp, M. Gather, B. Agnarsson, I. Sokolov, M. Miljkovic, S. Kéna-Cohen and S.A. Maier for their contributions to this work and useful discussions.

Optical Materials EXPRESS

Disclosures

The authors declare that there are no conflicts of interest related to this article.

References

1. M. Faraday, "Experimental relations of gold (and other metals) to light," Philos. Trans. R. Soc. Lond. **147**(0), 145–181 (1857).
2. W. R. Grove, "On the electro-chemical polarity of gases," Philos. Trans. R. Soc. Lond. **142**(0), 87–101 (1852).
3. O. S. Heavens, *Optical Properties of Thin Solid Films* (Butterworths Scientific Publications, 1955).
4. M. L. Brongersma and V. M. Shalaev, "Applied physics. The case for plasmonics," Science **328**(5977), 440–441 (2010).
5. J. B. Khurgin, "Replacing noble metals with alternative materials in plasmonics and metamaterials: how good an idea?" Philos Trans A Math Phys Eng Sci **375**(2090), 20160068 (2017).
6. A. V. Kildishev, A. Boltasseva, and V. M. Shalaev, "Planar photonics with metasurfaces," Science **339**(6125), 1232009 (2013).
7. J.-S. Huang, V. Callegari, P. Geisler, C. Brüning, J. Kern, J. C. Prangsma, X. Wu, T. Feichtner, J. Ziegler, P. Weinmann, M. Kamp, A. Forchel, P. Biagioni, U. Sennhauser, and B. Hecht, "Atomically flat single-crystalline gold nanostructures for plasmonic nanocircuitry," Nat. Commun. **1**(9), 150 (2010).
8. H. Qian, Y. Xiao, and Z. Liu, "Giant Kerr response of ultrathin gold films from quantum size effect," Nat. Commun. **7**(1), 13153 (2016).
9. R. Malureanu and A. Lavrinenko, "Ultra-thin films for plasmonics: a technology overview," Nanotechnol. Rev. **4**(3), 259–275 (2015).
10. D. S. Ghosh, "Ultrathin Metal Transparent Electrodes for the Optoelectronics Industry," Springer Theses, (2013)
11. R. S. Sennett and G. D. Scott, "The structure of evaporated metal films and their optical properties," J. Opt. Soc. Am. **40**(4), 203–211 (1950).
12. V. Krachmalnicoff, E. Castanié, Y. De Wilde, and R. Carminati, "Fluctuations of the local density of states probe localized surface plasmons on disordered metal films," Phys. Rev. Lett. **105**(18), 183901 (2010).
13. S. M. Novikov, J. Beermann, C. Frydendahl, N. Stenger, V. Coello, N. A. Mortensen, and S. I. Bozhevolnyi, "Enhancement of two-photon photoluminescence and SERS for low-coverage gold films," Opt. Express **24**(15), 16743–16751 (2016).
14. S. M. Novikov, C. Frydendahl, J. Beermann, V. A. Zenin, N. Stenger, V. Coello, N. A. Mortensen, and S. I. Bozhevolnyi, "White Light Generation and Anisotropic Damage in Gold Films near Percolation Threshold," ACS Photonics **4**(5), 1207–1215 (2017).
15. P. Pavaskar, I.-K. Hsu, J. Theiss, W. Hsuan Hung, and S. B. Cronin, "A microscopic study of strongly plasmonic Au and Ag island thin films," J. Appl. Phys. **113**(3), 034302 (2013).
16. R. L. Olmon, B. Slovick, T. W. Johnson, D. Shelton, S.-H. Oh, G. D. Boreman, and M. B. Raschke, "Optical dielectric function of gold," Phys. Rev. B Condens. Matter Mater. Phys. **86**(23), 235147 (2012).
17. F. Javier García de Abajo, "Nonlocal Effects in the Plasmons of Strongly Interacting Nanoparticles, Dimers, and Waveguides," J. Phys. Chem. C **112**(46), 17983–17987 (2008).
18. W. Zhou, D. J. Mandia, S. T. Barry, and J. Albert, "Anisotropic effective permittivity of an ultrathin gold coating on optical fiber in air, water and saline solutions," Opt. Express **22**(26), 31665–31676 (2014).
19. C. A. Goss, D. H. Charych, and M. Majda, "Application of (3-mercaptopropyl)trimethoxysilane as a molecular adhesive in the fabrication of vapor-deposited gold electrodes on glass substrates," Anal. Chem. **63**(1), 85–88 (1991).
20. T. G. Habteyes, S. Dhuey, E. Wood, D. Gargas, S. Cabrini, P. J. Schuck, A. P. Alivisatos, and S. R. Leone, "Metallic adhesion layer induced plasmon damping and molecular linker as a nondamping alternative," ACS Nano **6**(6), 5702–5709 (2012).
21. J. Sukham, O. Takayama, A. V. Lavrinenko, and R. Malureanu, "High-Quality ultrathin gold layers with an APTMS adhesion for optimal performance of surface plasmon polariton-based devices," ACS Appl. Mater. Interfaces **9**(29), 25049–25056 (2017).
22. I. Doron-Mor, Z. Barkay, N. Filip-Granit, A. Vaskevich, and I. Rubinstein, "Ultrathin Gold Island Films on Silanized Glass. Morphology and Optical Properties," Chem. Mater. **16**(18), 3476–3483 (2004).
23. R. A. Maniyara, D. Rodrigo, R. Yu, J. Canet-Ferrer, D. S. Ghosh, R. Yongsunthon, D. E. Baker, A. Rezikyan, F. J. García de Abajo, and V. Pruneri, "Tunable plasmons in ultrathin metal films," arXiv:1809.01449 [cond-mat.mes-hall].
24. M. Woehrmann and M. Toepper, "Polymerization of Thin Film Polymers," in *New Polymers for Special Applications* (Ailton De Souza Gomes, IntechOpen, 2012). DOI: 10.5772/48205.
25. K. Leosson, A. S. Ingason, B. Agnarsson, A. Kossoy, S. Olafsson, and M. C. Gather, "Ultra-thin gold films on transparent polymers," Nanophotonics **2**(1), 3–11 (2013).
26. A. Kossoy, V. Merk, D. Simakov, K. Leosson, S. Kéna-Cohen, and S. A. Maier, "Optical and Structural Properties of Ultra□thin Gold Films," Adv. Opt. Mater. **3**(1), 71–77 (2015).
27. I. Slovinsky, G. K. Stefansson, A. Kossoy, and K. Leosson, "Propagation Loss of Long-Range Surface Plasmon Polariton Gold Stripe Waveguides in the Thin-Film Limit," Plasmonics **8**(4), 1613–1619 (2013).
28. K. A. Willets and R. P. Van Duyne, "Localized surface plasmon resonance spectroscopy and sensing," Annu. Rev. Phys. Chem. **58**(1), 267–297 (2007).

Optical Materials EXPRESS

29. L. Gunnarsson, E. J. Bjerneld, H. Xu, S. Petronis, B. Kasemo, and M. Käll, "Interparticle coupling effects in nanofabricated substrates for surface-enhanced Raman scattering," Appl. Phys. Lett. **78**(6), 802–804 (2001).
30. Y. Fang, N.-H. Seong, and D. D. Dlott, "Measurement of the distribution of site enhancements in surface-enhanced Raman scattering," Science **321**(5887), 388–392 (2008).
31. V. Merk, J. Kneipp, and K. Leosson, "Gap size reduction and increased SERS enhancement in lithographically patterned nanoparticle arrays by templated growth," Adv. Opt. Mater. **1**(4), 313–318 (2013).
32. W. Ostwald, "Studien über die Bildung und Umwandlung fester Körper," Z. Phys. Chem. **22**(1), 289–330 (1897).
33. M. S. Schmidt, J. Hübner, and A. Boisen, "Large area fabrication of leaning silicon nanopillars for surface enhanced Raman spectroscopy," Adv. Mater. **24**(10), OP11–OP18 (2012).
34. P. Joshia and V. Santhanam, "Paper-based SERS active substrates on demand," RSC Advances **6**(72), 68545–68552 (2016).
35. S. M. Asiala and Z. D. Schultz, "Characterization of hotspots in a highly enhancing SERS substrate," Analyst (Lond.) **136**(21), 4472–4479 (2011).
36. K. Kneipp, A. S. Haka, H. Kneipp, K. Badizadegan, N. Yoshizawa, C. Boone, K. E. Shafer-Peltier, J. T. Motz, R. R. Dasari, and M. S. Feld, "Surface-enhanced Raman spectroscopy in single living cells using gold nanoparticles," Appl. Spectrosc. **56**(2), 150–154 (2002).
37. X. Cao, Y. Shan, L. Tan, X. Yu, M. Bao, W. Li, and H. Shi, "Hollow Au nanoflower substrates for identification and discrimination of the differentiation of bone marrow mesenchymal stem cells by surface-enhanced Raman spectroscopy," J. Mater. Chem. B Mater. Biol. Med. **5**(30), 5983–5995 (2017).
38. X. Sun and H. Li, "Gold nanoisland arrays by repeated deposition and post-deposition annealing for surface-enhanced Raman spectroscopy," Nanotechnology **24**(35), 355706 (2013).